ACS OMEGA

http://pubs.acs.org/journal/acsodf

Article

Highly Efficient Messenger RNA Transfection of Hard-to-Transfect Cells using Carbon Nanodots

Hojeong Shin and Dal-Hee Min*

Cite This: *ACS Omega* 2023, 8, 29113−29121

Read Online

ACCESS | Metrics & More | Article Recommendations | Supporting Information

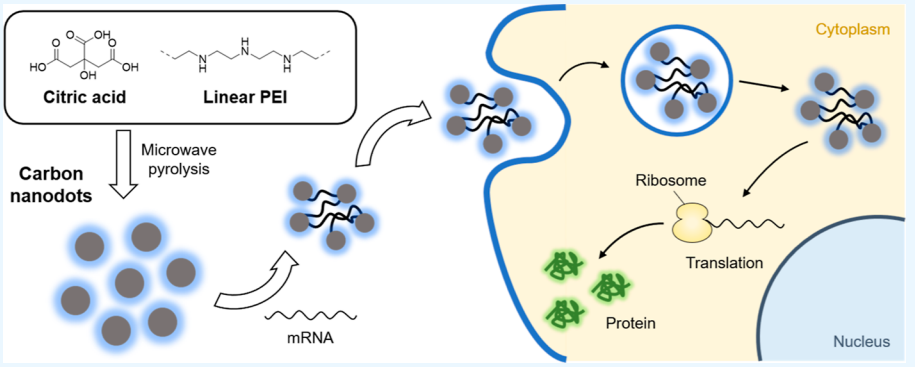

ABSTRACT: Although messenger RNA (mRNA)-based therapeutics opened up new avenues for treating various diseases, intracellular delivery of mRNA is still challenging, especially to hard-to-transfect cells. For successful mRNA therapy, the development of a delivery vehicle that can effectively transport mRNA into cells is essential. In this study, we synthesized carbon nanodots (CNDs) as an efficient mRNA delivery vehicle via a one-step microwave-assisted method. CNDs easily formed complexes with mRNA molecules by electrostatic interactions, and the gene delivery performance of CNDs was highly effective in hard-to-transfect cells. Considering their outstanding transfection ability, CNDs are expected to be further applied for mRNA-based cellular engineering.

INTRODUCTION

Over the past decades, gene therapy has received considerable attention as a promising strategy for treating numerous diseases.[1,2] Gene therapy aims to modify or regulate the expression of genes by introducing exogenous genetic material into target cells or tissues. Messenger RNA (mRNA) has recently gained attention as a promising class of drugs due to its ability to provide a transient source of gene expression without the risk of genomic integration, the need for nuclear localization or transcription, and relatively simple and cost-effective production.[3−5]

However, one of the significant challenges in mRNA-based gene therapy is delivering the genetic material into cells efficiently. Naked mRNA molecules are susceptible to serum nucleases and cannot efficiently penetrate the cell membrane, which limits their effectiveness as therapeutic agents. Therefore, efficient delivery systems that protect and deliver genetic materials safely into cells are essential for successful gene therapy.[6,7]

Currently, there are several mRNA delivery vehicle tools available, including lipid-based nanoparticles and viral vectors.[8,9] Lipid-based nanoparticles (LNPs) are widely used for mRNA delivery due to their ability to protect nucleic acids from degradation and facilitate cellular uptake. However, they exhibit some weaknesses for clinical applications because of their physiological instability, high toxicity, and low encapsulation efficiency.[10] LNPs have various stability issues upon storage, such as aggregation, gelation, leakage of encapsulated components, and unstable release profile.[11] Viral vectors, such as lentivirus and adeno-associated virus (AAV), are also efficient delivery systems, but they are associated with safety concerns, such as immunogenicity and potential integration into the host genome.[12−14]

Carbon nanodots (CNDs) have drawn attention in the nanobiotechnology field because of their outstanding physicochemical properties.[15−18] CNDs are easily prepared and exhibit good biocompatibility, colloidal stability, controllable surface functionality, and stable photoluminescence (PL). However, unmodified CNDs cannot efficiently load genetic material, and surface passivation with appropriate functions is

Received: April 1, 2023
Accepted: July 21, 2023
Published: August 2, 2023

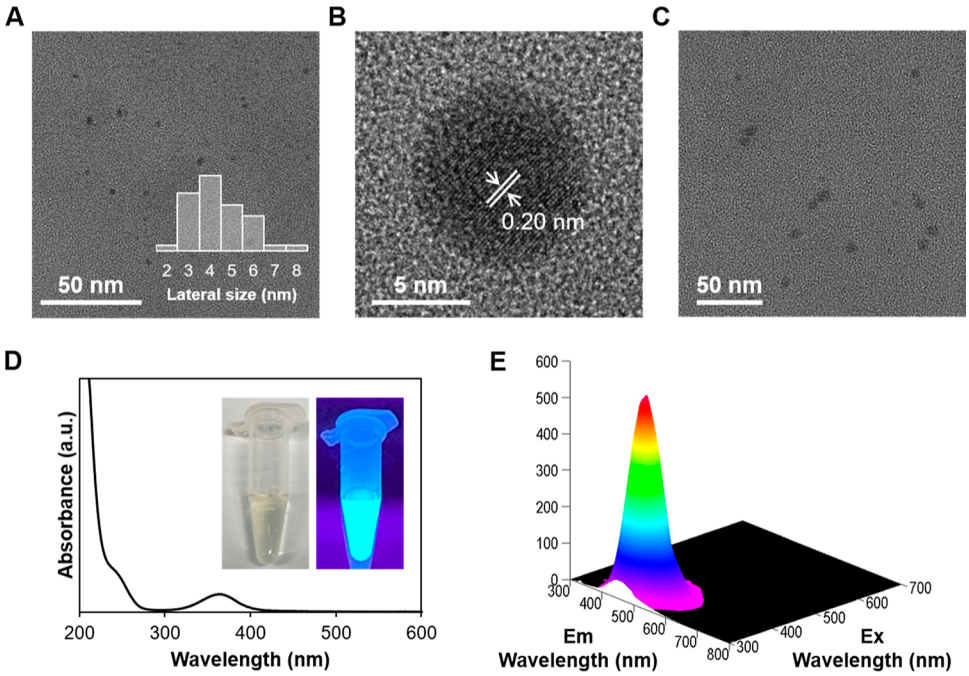

Figure 1. Characterization of CNDs. (A) HR-TEM image of CNDs, with the inset displaying the lateral size distribution of CNDs analyzed using ImageJ. (B) TEM image of individual CND with lattice fringes. (C) TEM image of the mRNA−CNDs complex. (D) UV−vis absorption spectrum of CNDs, with the inset showing photographic images of CNDs in an aqueous solution under daylight (left) and UV light (right) excited at 360 nm. (E) 3D excitation−emission matrix fluorescence spectrum of CNDs in an aqueous solution.

essential to improve their gene-binding ability.[17,18] In this regard, polyethyleneimine (PEI), a highly cationic polymer consisting of numerous amino groups, can serve as a surface passivation agent on CNDs for gene delivery.

Although several strategies have been proposed to improve the efficiency of mRNA delivery, one of the main challenges that remains is delivering mRNA to hard-to-transfect cells, such as immune cells.[19,20] Recent successes in cancer immunotherapy, including complete remission of refractory acute lymphoblastic leukemia (ALL) using chimeric antigen receptor (CAR)-engineered T cells[21] and efficient treatment of malignant melanoma with adoptive cell therapy (ACT),[22] highlight the potential for mRNA delivery to revolutionize the field. Therefore, delivering mRNA to immune cells could have significant clinical implications for cancer immunotherapy.

In this context, the current study aims to develop a novel mRNA delivery system based on CNDs and demonstrate its high transfection efficiency in delivering mRNA into hard-to-transfect cells. We synthesized CNDs as an efficient gene delivery platform employing a straightforward microwave-assisted pyrolysis method with citric acid and 25 kDa linear polyethyleneimine (PEI_{25k}). Through electrostatic interactions, the cationic CNDs effectively bind to anionic nucleic acids. Importantly, we successfully demonstrated the remarkable transfection efficiency of CNDs in delivering mRNA into various cell types that are traditionally difficult to transfect, including macrophages, lymphocytes, and leukemia cell lines.

RESULTS AND DISCUSSION

Characterization of CNDs. High-resolution transmission electron microscopy (HR-TEM) images revealed the successful synthesis of CNDs. The CNDs exhibited a lateral dimension ranging from 2 to 8 nm, with an average size of 3.78 ± 1.21 nm (Figure 1A) and the lattice fringes with a *d*-spacing of 0.20 nm (Figure 1B). TEM imaging of the mRNA-loaded CNDs demonstrated their uniform distribution and exhibited a spherical morphology (Figure 1C). The UV−vis spectrum of CNDs showed a shoulder at 230 nm assigned to the $\pi \rightarrow \pi^*$ transitions of the aromatic C═C bonds and an absorption peak at around 360 nm corresponding to $n \rightarrow \pi^*$ transitions of the C═O bonds (Figure 1D).[23]

CNDs showed good dispersion in an aqueous solution with a zeta potential of +13.6 ± 1.9 mV at pH 7.4 and emitted blue light under UV irradiation at 360 nm (Figure 1D). Figure 1E shows a three-dimensional plot of the excitation−emission matrix fluorescence spectrum of CNDs. The spectrum of CNDs is characterized by a peak at a maximum emission of around 450 nm under excitation at 360 nm. The quantum yield (QY) of CNDs was determined using the comparative method which employs quinine sulfate as a standard, resulting in a QY value of 27.1%. We conducted a photostability assessment of the CNDs by exposing them to UV light for varying durations. The CNDs retained approximately 83.6% of their initial emission intensity, even after prolonged UV exposure of up to 4 h (Figure S1).

The X-ray photoelectron spectroscopy (XPS) analysis of CNDs indicated the presence of carbon (C 1s, 284.9 eV), nitrogen (N 1s, 399.9 eV), and oxygen (O 1s, 531.9 eV) (Figure S2A).[24−26] The deconvoluted high-resolution XPS spectra of C 1s identified distinct peaks attributed to C═C (284.5 eV), C−N (285.7 eV), C−O (287.4 eV), and C═O (288.2 eV) bonds (Figure S2B). Furthermore, the high-resolution N 1s spectra demonstrated that the nitrogen in CNDs existed as C−N−C (399.5 eV) and N−H (401.1 eV) forms (Figure S2C). These results indicate the successful preparation of CNDs. These results indicate the successful preparation of CNDs.

Before investigating gene delivery performance, we evaluated the loading capacity of CNDs to mRNA. Nucleic acids and

https://doi.org/10.1021/acsomega.3c01394
ACS Omega 2023, 8, 29113−29121

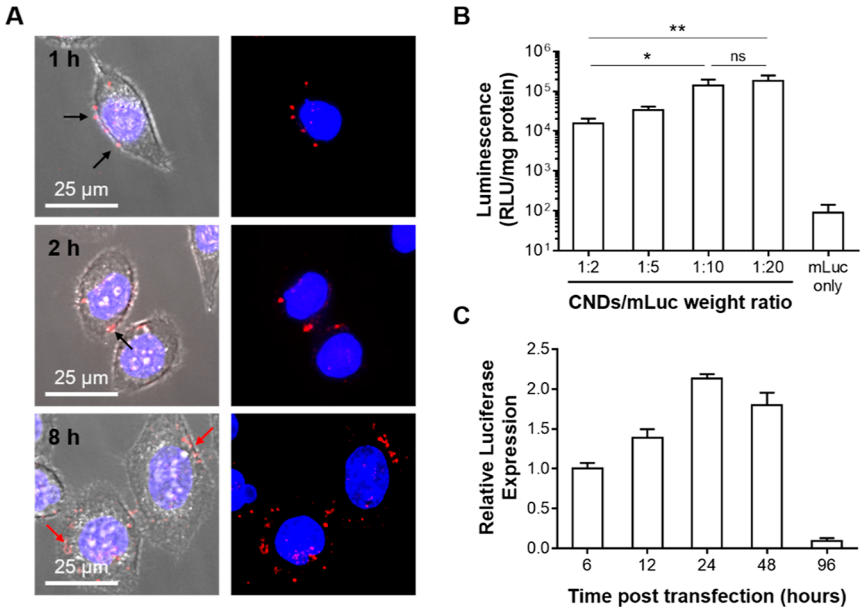

Figure 2. (A) Cellular uptake of mRNA−CNDs. Red fluorescence signals from AF647-labeled mRNA in HeLa cells treated with mRNA−CNDs for 1, 2, and 8 h. (B) Optimization of CNDs/mLuc weight ratio by measuring the luciferase expression in HeLa cells transfected with mLuc−CNDs complexes with different weight ratios. (C) Luciferase expression over time in HeLa cells transfected with mLuc−CNDs complexes, with results normalized to expression at 6 h.

CNDs can readily form complexes in an aqueous solution via electrostatic interactions. A gel retardation assay was conducted to evaluate the loading capacity (Figure S3A). mRNA−CNDs complexes were prepared at different weight ratios. mRNA molecules completely lost their mobility in the 1% agarose gel at a CNDs/mRNA weight ratio of 2. The zeta potential of CNDs decreased to +1.2 ± 0.9 mV at pH 7.4 after mixing with mRNA. The hydrodynamic size of the CNDs was measured using dynamic light scattering (DLS) both before and after combination with mRNA. The analysis revealed that the CNDs had diameters ranging from 2 to 10 nm (Figure S3B), while the mRNA−CNDs nanocomplexes had diameters ranging from 10 to 30 nm (Figure S3C). These data suggest the successful formation of complexes between genetic payloads and CNDs. We also investigated the stability of both CNDs and mRNA−CNDs in serum-free media at 37 °C for 24 h. After incubation, there were no discernible changes in the size diameters of either CNDs or mRNA−CNDs, indicating that both were highly stable under these conditions (Figure S3D).

In addition, low cytotoxicity is a necessary requirement for a feasible gene delivery carrier. To evaluate in vitro cytotoxicity of CNDs, the cell viability was determined via CCK-8 assay (Figure S4). HeLa, K562, U937, and Raw264.7 cells were incubated with various concentrations of free PEI_{25k} or CNDs for 24 h. In all cell lines, CNDs exhibited higher cell viability than PEI_{25k}, as demonstrated by the CCK-8 assay. The low cytotoxicity of CNDs may be attributed to the decreased density of amine groups during the passivation process.[17]

Cellular Uptake of mRNA−CNDs Complexes. After confirming the successful loading of mRNA, we sought to investigate the cellular uptake of the mRNA−CNDs complexes. To visualize cellular uptake, mRNA molecules were labeled with the fluorescent dye Alexa Fluor 647 (AF647) and mixed with CNDs. AF647-labeled mRNA−CNDs complexes were treated to HeLa cells, and cellular uptake was monitored using fluorescence microscopy (Figure 2A). For 2 h after treatment, the complexes could be seen attached to the surface of the cells (black arrow). At 8 h post-treatment, a red fluorescence signal originating from AF647-labeled mRNA was abundantly observed in the cytoplasm at 8 h (red arrow), indicating successful endocytosis of mRNA−CNDs.

In order to compare the cellular uptake of CNDs and PEI_{25k}, we assessed the median fluorescence intensity (MFI) through flow cytometry analysis (Figure S5). Specifically, we mixed AF647-labeled mRNA with either CNDs or PEI_{25k} and administered the resulting mixture to HeLa cells. Subsequently, we analyzed the MFI of each cell at 24 h post-treatment to determine the extent of cellular uptake. Our results demonstrated that the CND group exhibited significantly higher fluorescence compared to the PEI_{25k} group, indicating a greater degree of cellular uptake. This may be attributed to the smaller size of CNDs, which facilitates their penetration through the cell membrane.[27]

Efficiency of CNDs for mRNA Transfection in HeLa Cells. Having confirmed the cellular uptake of mRNA−CNDs complexes, we sought to evaluate the mRNA delivery capability of CNDs in HeLa cells (human cervical carcinoma cell line). Cells were incubated with firefly luciferase-encoding mRNA (mLuc)−CNDs complex. First, we optimized the weight ratio of CNDs/mLuc for effective transfection. To determine the optimal CNDs/mLuc ratio for transfecting HeLa cells in a 24-well plate, the amount of mLuc was fixed to 0.1 μg and the amount of CNDs was changed from 1 to 10 μg. The transfection efficiency was measured by luciferase enzyme activity 24 h after the treatment. Although mRNA is fully complexed at a CNDs/mRNA weight ratio of 2, transfection efficiencies increased at higher weight ratios (Figure 2B) because the weight ratio affects the characteristics of mRNA−CNDs complexes such as size and charge that are determining factors in gene transfection.[28−30] Therefore, we chose the CNDs/nucleic acids with a weight ratio of 10 in the following experiments. Next, we verified the luciferase expression kinetics

https://doi.org/10.1021/acsomega.3c01394
ACS Omega 2023, 8, 29113−29121

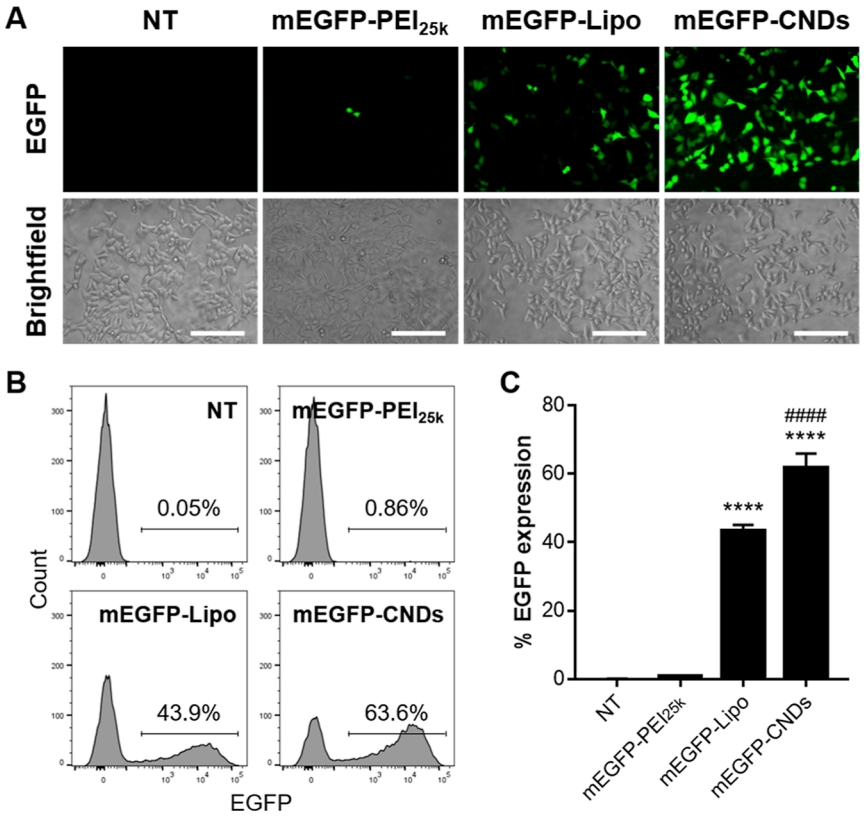

Figure 3. Analysis of mRNA transfection efficiency using mEGFP in HeLa cells. (A) Optical observation of the EGFP expression, with representative fluorescence microscopic images of each group: NT control, mEGFP complexed with PEI_{25k} (mEGFP−PEI_{25k}), mEGFP complexed with Lipo (mEGFP−Lipo), and mEGFP loaded on CNDs (mEGFP−CNDs). The scale bar represents 100 μm. (B) Representative histogram and (C) quantitative plot of flow cytometry analysis for EGFP expression in HeLa cells. Data are presented as mean with SD (n = 4 per group). Statistical significance was determined using one-way ANOVA, and the comparison of mEGFP−Lipo and mEGFP−CNDs to mEGFP−PEI_{25k} is indicated by asterisks (****P < 0.0001), and the differences between mEGFP−Lipo and mEGFP−CNDs are indicated by hashtags ($^{\#\#\#\#}P$ < 0.0001).

upon the transfection of mLuc using CNDs. The luminescence signal in HeLa cells increased over time until 24 h, suggesting transient expression of luciferase (Figure 2C). The signal decreased after 24 h and was barely measurable at 96 h; therefore, we used 24 h time point for the following experiments.

We then compared the transfection efficiency of CNDs with that of PEI_{25k} and Lipofectamine 2000 (Lipo) using EGFP mRNA (mEGFP). HeLa cells were treated with 0.1 μg of mEGFP in a 24-well plate. After 24 h of transfection, we observed the cells with fluorescence microscopy to examine the EGFP expression (Figure 3A). HeLa cells treated with the mEGFP−CNDs group showed notably increased EGFP expression compared to cells treated with the mEGFP−PEI_{25k} polyplex. Moreover, the mEGFP−CNDs group showed higher fluorescence signal compared to the group using Lipo, the gold standard among transfection reagents. To quantify the transfection efficiencies of each group, we used flow cytometry analysis (Figure 3B,C). The overall tendency of flow cytometry results showed a decent correlation with fluorescence imaging. Based on flow cytometry results, the EGFP expression of the mEGFP−CNDs group (61.8%) was 1.4-fold higher than that of the mEGFP−Lipo group (43.3%).

Additionally, we examined the impact of increasing the mRNA dose to 2 μg/well on transfection efficiency (Figure S6). In the PEI_{25k} group, the higher mRNA dose led to an increase in transfection efficiency; however, this improvement came at the expense of decreased cell viability due to the inherent high toxicity associated with PEI at elevated concentrations. In contrast, the utilization of CNDs, which exhibit low toxicity, maintained a consistently high cell viability even when subjected to high mRNA doses, while concurrently achieving remarkable transfection efficiency.

mRNA−CNDs Complex-Mediated Transfection in Hard-to-Transfect Cells. The mRNA delivery efficiency was further studied in hard-to-transfect cells. First, Raw264.7 cells (murine macrophage cell line) were transfected with 1 μg of mEGFP in a 24-well plate (Figure 4A). Exposure of cells to the mEGFP−CNDs achieved significantly high gene expression rates of 16.9%, which is 3.2-fold higher than that mediated by Lipo (Figure 4B,C).

Next, cultured K562 cells (human chronic myelogenous leukemia cell line) were treated with different formulations of mEGFP. Observed with an optical microscope, the mEGFP−CNDs group displayed a significant mRNA transfection efficacy, higher than the mEGFP−PEI_{25k} and mEGFP−Lipo groups (Figure 4D). Quantification by flow cytometry confirmed that the frequency of EGFP-positive cells among K562 cells transfected with mEGFP−CNDs (73.2%) was 3.1-fold higher than that transfected with mEGFP−Lipo (23.7%) (Figure 4E,F). When assessed by the MFI, cells treated with mEGFP−CNDs showed the most significant gene expression.

For further validation, U937 cells (human histiocytic lymphoma cell line) were tested and showed efficient

https://doi.org/10.1021/acsomega.3c01394
ACS Omega 2023, 8, 29113−29121

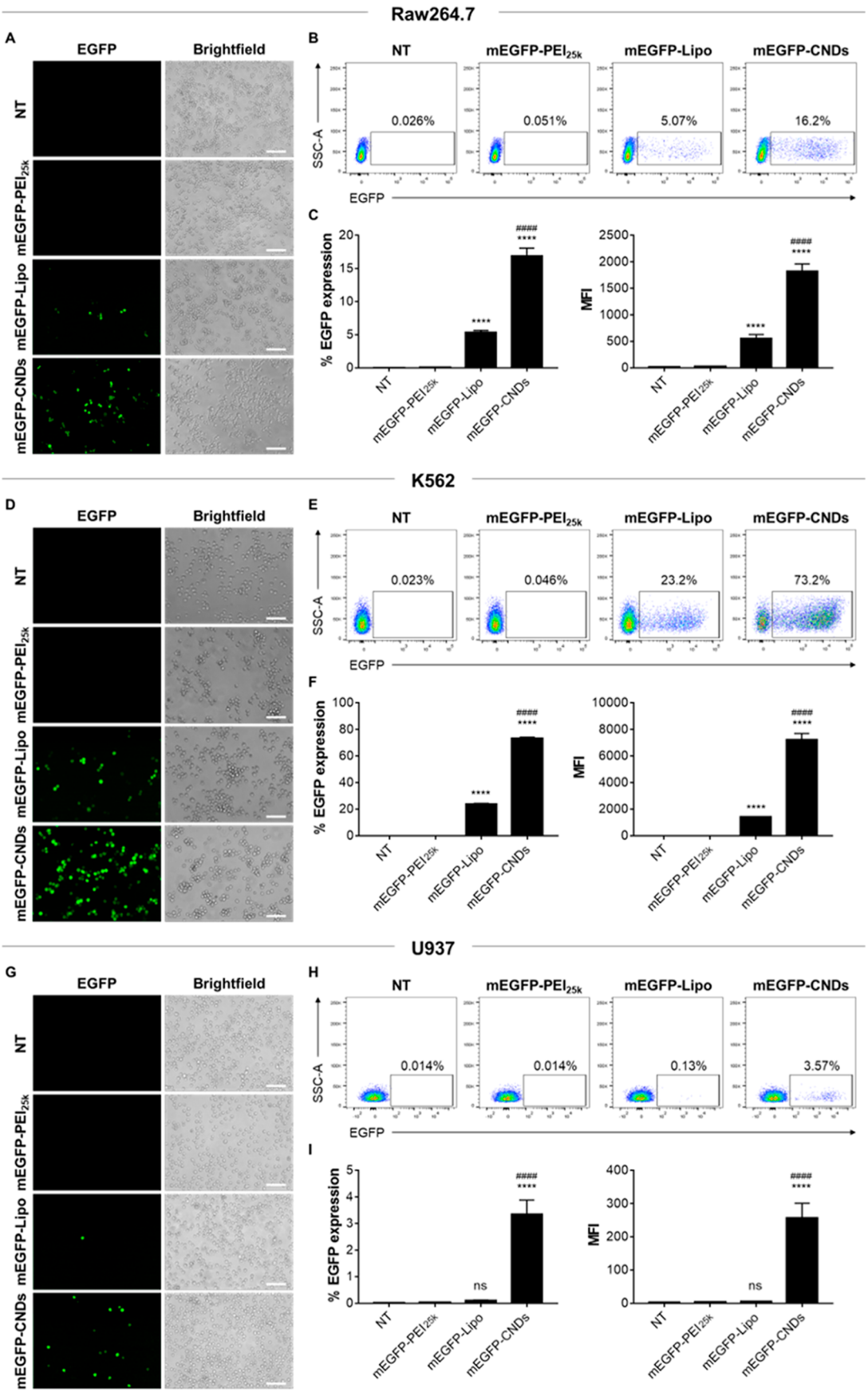

Figure 4. Analysis of mRNA transfection efficiency in Raw264.7 cells (A−C), K562 cells (D−F), and U937(G−I). (A) Optical observation of the EGFP expression in Raw264.7 cells, with representative fluorescence microscopic images of each group: NT control, mEGFP complexed with PEI_{25k} (mEGFP−PEI_{25k}), mEGFP complexed with Lipo (mEGFP−Lipo), and mEGFP loaded on CNDs (mEGFP−CNDs). The scale bar

https://doi.org/10.1021/acsomega.3c01394
ACS Omega 2023, 8, 29113−29121

Figure 4. continued

represents 100 μm. (B) Representative dot plot and (C) quantitative plot of flow cytometry analysis for EGFP expression in Raw264.7 cells. (D) Optical observation of the EGFP expression in K562 cells, with representative fluorescence microscopic images of each group. The scale bar represents 100 μm. (E) Representative dot plot and (F) quantitative plot of flow cytometry analysis for EGFP expression in K562 cells. (G) Optical observation of the EGFP expression in U937 cells, with representative fluorescence microscopic images of each group. The scale bar represents 100 μm. (H) Representative dot plot (I) and quantitative plot of flow cytometry analysis for EGFP expression in U937 cells. Data are presented as mean with SD (n = 4 per group). Statistical significance was determined using one-way ANOVA, and the comparison of mEGFP−Lipo and mEGFP−CNDs to mEGFP−PEI_{25k} is indicated by asterisks (ns: not significant and ****$P < 0.0001$), and the differences between mEGFP−Lipo and mEGFP−CNDs are indicated by hashtags ($^{\#\#\#\#}P < 0.0001$).

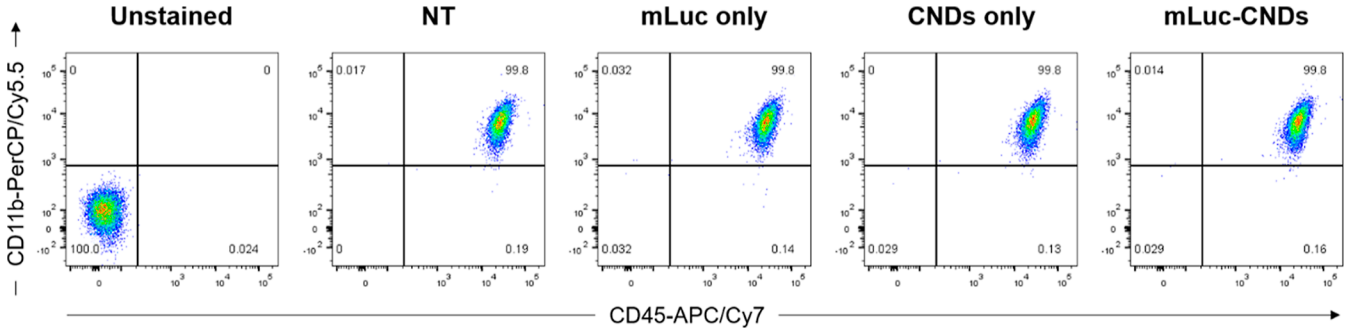

Figure 5. Effect of CNDs-based mRNA transfection on expression levels of cell surface markers on Raw264.7 cells. Cells were treated with mLuc alone, CNDs alone, or mLuc−CNDs complexes. NT cells were used as a control. After 24 h post-treatment, cells were stained for CD45 and CD11b and quantified using flow cytometry.

transfection of mRNA via mEGFP−CNDs through both fluorescence microscopy and flow cytometry (Figure 4G,H). Interestingly, there were no statistical differences between the EGFP-positive cell population of nontransfected cells (0.02%) and cells treated with mEGFP−Lipo (0.10%) (Figure 4I). However, treatment with mEGFP−CNDs achieved significantly high cell transfection (3.34%) and MFI compared to treatment with mEGFP−Lipo. Taken together, these results demonstrate that CNDs are efficient transfection agents for mRNA delivery in hard-to-transfect cells.

In addition, we investigated changes in the expression levels of cell surface markers to measure the cytotoxicity of mLuc−CNDs in immune cells. Raw264.7 cells were treated with mLuc alone, CNDs alone, and mLuc−CNDs complexes. After each treatment for 24 h, the cells were stained for CD45 and CD11b, common cell surface markers utilized to recognize macrophages. As shown in Figure 5, there was no significant change in the expression of CD45 and CD11b.

siRNA and pDNA Delivery using CNDs. To demonstrate the broad applicability of our platform, we evaluated whether CNDs could be utilized as delivery carriers for siRNA and pDNA. We first assessed the gene knockdown efficiency of CNDs complexed with siRNA targeting GFP (siGFP). The siGFP−CNDs complex was tested in GFP-expressing HeLa (GFP−HeLa) cells. As shown in Figure S7A, treatment with siGFP−CNDs significantly decreased GFP fluorescence in GFP−HeLa cells. A flow cytometry analysis was performed to quantify the gene knockdown efficiency (Figure S7B). The proportion of GFP-positive cells was 95.43% in nontransfected GFP−HeLa cells. On the other hand, in the siGFP−CNDs-treated GFP-HeLa cells, the percentage of GFP-positive cells decreased down to 37.75%, which is lower than that in siGFP−PEI_{25k} (90.84%) and siGFP−Lipo (47.88%)-treated GFP−HeLa cells. Taken together, these results demonstrate the great potential of CNDs as a highly efficient gene vector for siRNA delivery as well as mRNA delivery.

The suitability of CNDs for pDNA delivery was further investigated. The intracellular delivery of RFP pDNA (pRFP) was conducted by incubating HeLa cells with pRFP−PEI_{25k}, pRFP−Lipo, and pRFP−CNDs. pRFP expression was analyzed by fluorescence microscopy and both Lipo and CNDs groups exhibited the RFP expression in cells (Figure S7C). The expressed RFP level was also quantified by flow cytometry analysis (Figures S7D). The quantitative results from flow cytometry were consistent with the fluorescence images. Flow cytometry results showed that there was no significant difference in the pDNA transfection efficacy between Lipo and CNDs groups, while both were significantly higher than PEI_{25k}. These results provide evidence that CNDs are a suitable delivery platform for not only mRNA molecules but also siRNA and pDNA.

CONCLUSIONS

In this work, we synthesized CNDs via the one-pot microwave-assisted method. Positively charged CNDs and negatively charged genetic payloads formed stable complexes under physiological conditions. We used mRNA−CNDs complexes to transfect several types of mammalian cell lines. CNDs achieved highly efficient mRNA delivery into hard-to-transfect cells (macrophage, lymphocyte, and leukemia cell lines), and CNDs exhibited notably higher performance for mRNA transfection compared to the standard transfection agent, Lipofectamine 2000. Future research will be needed to demonstrate the utility of CNDs for therapeutic applications. Notably, due to their high transfection efficiency in immune cells, CNDs might be utilized for mRNA-based immune cell engineering. For example, mRNA-based approaches using CNDs could potentially be used to deliver genes encoding tumor-specific T cell receptors (TCRs) or CARs into lymphocytes, allowing for more precise targeting of cancer cells and potentially reducing off-target effects. We anticipate that CNDs may facilitate the development of gene therapies

https://doi.org/10.1021/acsomega.3c01394
ACS Omega 2023, 8, 29113−29121

and cell therapies after further studies on preclinical applications.

MATERIALS AND METHODS

Materials. Citric acid was purchased from Sigma-Aldrich. Linear PEI (25 kDa) was purchased from Polysciences, Inc. DMEM (Dulbecco's modified Eagle's medium), 0.25% trypsin−EDTA solution, PBS (pH 7.4), FBS, and P/S were purchased from WelGENE Inc. CCK-8 (cell counting kit-8) was purchased from Dojindo Molecular Technologies, Inc. CleanCap FLuc mRNA and CleanCap EGFP mRNA were purchased from TriLink Biotechnologies. GFP siRNA was purchased from Bioneer. Recombinant plasmid encoding RFP was purchased from Addgene. APC/Cy7 anti-mouse CD45 and PerCP/Cy5.5 anti-mouse CD11b were purchased from Biolegend.

Synthesis of CNDs. CNDs were synthesized according to the microwave-assisted hydrothermal approach. Citric acid (150 mg) and linear PEI (50 mg) were mixed in 10 mL of distilled water. After sonication, the transparent solution was placed into a microwave (1000 W). The hydrothermal reaction was repeated until the reaction solution turned yellow. The solution was filtered with an Amicon filter (Merck Millipore) and dialyzed for 3 days. Purified CNDs were freeze-dried and dispersed in DI water. A production yield of 31.6 wt % was obtained for the synthesis of CNDs.

Characterization of CNDs. The TEM images were acquired using a JEM-F200 (JEOL Ltd.), and the size distribution of CNDs was analyzed with ImageJ software. The UV−vis absorbance of CNDs was obtained by the S-3100 (Scinco). 3D fluorescence spectra of CNDs were obtained with a spectrofluorometer FP-8300 (JASCO). Zeta potential and hydrodynamic size were measured using a Zetasizer Nano S (Malvern Panalytical). XPS analysis was performed on an Axis Supra (Kratos) installed at the National Center for Inter-university Research Facilities (NCIRF) at Seoul National University.

QY Calculation. We determined the QY of the sample relative to quinine sulfate in 0.1 M H_2SO_4 using the following formula.[31]

$$Q_S = Q_R \times \frac{I_S}{I_R} \times \frac{A_R}{A_S} \times \frac{\eta_S^2}{\eta_R^2}$$

where Q_S is the QY of the sample, Q_R is the QY of the reference, I_S is the area under the PL curve of the sample, I_R is the area under the PL curve of the reference, A_S is the absorbance of the sample, A_R is the absorbance of the reference, η_S is the refractive index of the sample, and η_R is the refractive index of the reference.

Gel Retardation Assay. The loading capacity of CNDs to mRNA, siRNA, and pDNA was analyzed by agarose gel electrophoresis. One hundred nanograms of mRNA, siRNA, and pDNA was mixed with various amounts of CNDs in PBS for 30 min. The samples were added with LoadingStar (Dyne Bio Inc.) and loaded on 1% agarose gel. After running the gel, it was analyzed with a ChemiDoc Imaging System (Bio-Rad).

Cell Viability Test. The CCK-8 assay was performed according to the manufacturer's instructions. HeLa, Raw264.7, K562, and U937 cells were seeded in 96-well culture plates. After overnight incubation, the cells were treated with CNDs in serially diluted concentrations for 24 h. The cells were rinsed with 1× PBS twice, and the CCK-8 reagent was treated at a concentration of 10% (v/v) and incubated for 1 h. The optical density at 450 nm was measured by SynergyMx (Biotek) in the absorbance mode.

Luciferase Assay. HeLa cells were seeded onto 24-well culture plates at a density of 5×10^5 cells per well and incubated with DMEM supplemented with 10% FBS and P/S. After overnight incubation, the cells were briefly washed with 1× PBS. Next, 0.1 μg of mLuc was complexed with various amounts of CNDs. HeLa cells were treated with each complex in 0.5 mL of serum-free media. After 24 h of incubation, the cells were washed with 1× PBS and treated with trypsin−EDTA for 2 min. Collected cells were analyzed by the Luciferase Assay System (Promega) according to the manufacturer's instructions.

mEGFP Transfection. HeLa cells were seeded onto 24-well culture plates at a density of 5×10^4 cells per well and incubated with DMEM supplemented with 10% FBS and P/S. After overnight incubation, the cells were briefly washed with 1× PBS. Next, 0.1 μg per well of mEGFP was complexed with PEI_{25k}, Lipo, or CNDs. HeLa cells were treated with each complex in 0.5 mL of serum-free media.

Raw264.7, K562, and U937 cells were seeded onto 24-well culture plates at a density of 1×10^5 cells per well. Raw 264.7 cells were incubated with DMEM supplemented with 10% FBS and P/S. K562 and U937 cells were incubated with RPMI supplemented with 10% FBS. One microgram per well of mEGFP was complexed with PEI_{25k}, Lipo, or CNDs, and cells were treated with each complex in 0.5 mL of serum-free media. After 24 h of incubation, the cells were washed with 1× PBS and treated with trypsin−EDTA for 2 min. Collected cells were analyzed by FACSLyric (BD Biosciences).

siGFP and pRFP Transfection. For siRNA delivery, GFP−HeLa cells were seeded onto 24-well culture plates at a density of 5×10^4 cells per well and incubated with DMEM supplemented with 10% FBS and P/S. After overnight incubation, the cells were briefly washed with 1× PBS. Next, 10 pmole siGFP was complexed with PEI_{25k}, Lipo, or CNDs. HeLa cells were treated with 1× PBS, siGFP−PEI_{25k}, siGFP−Lipo, and siGFP−CNDs in 0.5 mL of serum-free media. After 24 h of incubation, the cells were washed with 1× PBS and treated with trypsin−EDTA for 2 min. Collected cells were analyzed by FACSLyric (BD Biosciences).

For pDNA transfection, HeLa cells were seeded onto 24-well culture plates at a density of 5×10^4 cells per well and incubated with DMEM supplemented with 10% FBS and P/S. After overnight incubation, the cells were briefly washed with 1× PBS. Next, 0.5 μg of pRFP was complexed with PEI_{25k}, Lipo, or CNDs. HeLa cells were treated with each complex in 0.5 mL of serum-free media. After 24 h of incubation, the cells were washed with 1× PBS and treated with trypsin−EDTA for 2 min. Collected cells were analyzed by FACSLyric (BD Biosciences).

Statistics. Statistical analysis was conducted using the GraphPad Prism software as described in the indicated figure legends. Statistical significance was assigned when the value of P was <0.05. Error bars and the number of n are indicated in the figure legends.

ASSOCIATED CONTENT

Supporting Information

The Supporting Information is available free of charge at https://pubs.acs.org/doi/10.1021/acsomega.3c01394.

https://doi.org/10.1021/acsomega.3c01394
ACS Omega 2023, 8, 29113−29121

Photostability evaluation of CNDs under continuous irradiation with UV light; XPS analysis of CNDs; gel retardation assay and stability test of CNDs; cytotoxicity of free PEI_{25k} and CNDs in HeLa, Raw264.7, K562, and U937 cells; cellular uptake assessment in HeLa cells following treatment of AF647-labeled mRNA mixed with either free PEI_{25k} or CNDs; silencing of GFP expression in GFP−HeLa cells using siGFP; and the analysis of pDNA transfection efficiency using pRFP in HeLa cells (PDF)

AUTHOR INFORMATION

Corresponding Author

Dal-Hee Min − *Department of Chemistry and Department of Biological Sciences, Seoul National University, Seoul 08826, Republic of Korea; Institute of Biotherapeutics Convergence Technology, Lemonex Inc., Seoul 06683, Republic of Korea;* orcid.org/0000-0001-8623-6716; Email: dalheemin@snu.ac.kr

Author

Hojeong Shin − *Department of Chemistry, Seoul National University, Seoul 08826, Republic of Korea;* orcid.org/0000-0001-5895-0955

Complete contact information is available at: https://pubs.acs.org/10.1021/acsomega.3c01394

Author Contributions

The manuscript was written through contributions of all authors.

Funding

This work was supported by the Basic Science Research Program through the National Research Foundation of Korea (NRF) funded by the Ministry of Science and ICT (2021R1A2B5B03086506) and Lemonex Inc. (LEMONEX-SN201901-3-30 and LEMONEX-SN202003-3-60).

Notes

The authors declare no competing financial interest.

REFERENCES

(1) Dunbar, C. E.; High, K. A.; Joung, J. K.; Kohn, D. B.; Ozawa, K.; Sadelain, M. Gene Therapy Comes of Age. *Science* **2018**, *359*, No. eaan4672.

(2) Bulaklak, K.; Gersbach, C. A. The Once and Future Gene Therapy. *Nat. Commun.* **2020**, *11*, 5820.

(3) Sahin, U.; Kariko, K.; Tureci, O. mRNA-Based Therapeutics - Developing a New Class of Drugs. *Nat. Rev. Drug Discovery* **2014**, *13*, 759−780.

(4) Pardi, N.; Hogan, M. J.; Porter, F. W.; Weissman, D. mRNA Vaccines - a New Era in Vaccinology. *Nat. Rev. Drug Discovery* **2018**, *17*, 261−279.

(5) Barbier, A. J.; Jiang, A. Y.; Zhang, P.; Wooster, R.; Anderson, D. G. The Clinical Progress of mRNA Vaccines and Immunotherapies. *Nat. Biotechnol.* **2022**, *40*, 840−854.

(6) Chen, J.; Guo, Z. P.; Tian, H. Y.; Chen, X. S. Production and Clinical Development of Nanoparticles for Gene Delivery. *Mol. Ther.–Methods Clin. Dev.* **2016**, *3*, 16023.

(7) Shin, H.; Park, S. J.; Yim, Y.; Kim, J.; Choi, C.; Won, C.; Min, D. H. Recent Advances in RNA Therapeutics and RNA Delivery Systems Based on Nanoparticles. *Adv. Ther.* **2018**, *1*, 1800065.

(8) Nayerossadat, N.; Ali, P.; Maedeh, T. Viral and Nonviral Delivery Systems for Gene Delivery. *Adv. Biomed. Res.* **2012**, *1*, 27.

(9) Sung, Y. K.; Kim, S. W. Recent Advances in the Development of Gene Delivery Systems. *Biomater. Res.* **2019**, *23*, 8.

(10) Lv, H. T.; Zhang, S. B.; Wang, B.; Cui, S. H.; Yan, J. Toxicity of Cationic Lipids and Cationic Polymers in Gene Delivery. *J. Controlled Release* **2006**, *114*, 100−109.

(11) Thi, T. T. H.; Suys, E. J. A.; Lee, J. S.; Nguyen, D. H.; Park, K. D.; Truong, N. P. Lipid-Based Nanoparticles in the Clinic and Clinical Trials: From Cancer Nanomedicine to Covid-19 Vaccines. *Vaccines* **2021**, *9*, 359.

(12) Thomas, C. E.; Ehrhardt, A.; Kay, M. A. Progress and Problems with the Use of Viral Vectors for Gene Therapy. *Nat. Rev. Genet.* **2003**, *4*, 346−358.

(13) Guan, S.; Rosenecker, J. Nanotechnologies in Delivery of mRNA Therapeutics Using Nonviral Vector-Based Delivery Systems. *Gene Ther.* **2017**, *24*, 133−143.

(14) Shim, G.; Kim, D.; Le, Q. V.; Park, G. T.; Kwon, T.; Oh, Y. K. Nonviral Delivery Systems for Cancer Gene Therapy: Strategies and Challenges. *Curr. Gene Ther.* **2018**, *18*, 3−20.

(15) Li, H. T.; Kang, Z. H.; Liu, Y.; Lee, S. T. Carbon Nanodots: Synthesis, Properties and Applications. *J. Mater. Chem.* **2012**, *22*, 24230−24253.

(16) Jaleel, J. A.; Pramod, K. Artful and Multifaceted Applications of Carbon Dot in Biomedicine. *J. Controlled Release* **2018**, *269*, 302−321.

(17) Kim, S.; Choi, Y.; Park, G.; Won, C.; Park, Y. J.; Lee, Y.; Kim, B. S.; Min, D. H. Highly Efficient Gene Silencing and Bioimaging Based on Fluorescent Carbon Dots in Vitro and in Vivo. *Nano Res.* **2017**, *10*, 503−519.

(18) Park, S. J.; Shin, H.; Won, C.; Min, D. H. Non-Viral, Direct Neuronal Reprogramming from Human Fibroblast Using a Polymer-Functionalized Nanodot. *Nanomed.: Nanotechnol. Biol. Med.* **2021**, *32*, 102316.

(19) Kumar, A. R. K.; Shou, Y.; Chan, B.; Krishaa, L.; Tay, A. Materials for Improving Immune Cell Transfection. *Adv. Mater.* **2021**, *33*, No. e2007421.

(20) Qin, S.; Tang, X.; Chen, Y.; Chen, K.; Fan, N.; Xiao, W.; Zheng, Q.; Li, G.; Teng, Y.; Wu, M.; Song, X. mRNA-Based Therapeutics: Powerful and Versatile Tools to Combat Diseases. *Signal Transduction Targeted Ther.* **2022**, *7*, 166.

(21) Grupp, S. A.; Kalos, M.; Barrett, D.; Aplenc, R.; Porter, D. L.; Rheingold, S. R.; Teachey, D. T.; Chew, A.; Hauck, B.; Wright, J. F.; Milone, M. C.; Levine, B. L.; June, C. H. Chimeric Antigen Receptor-Modified T Cells for Acute Lymphoid Leukemia. *N. Engl. J. Med.* **2013**, *368*, 1509−1518.

(22) Rosenberg, S. A.; Dudley, M. E. Adoptive Cell Therapy for the Treatment of Patients with Metastatic Melanoma. *Curr. Opin. Immunol.* **2009**, *21*, 233−240.

(23) Shin, H.; Park, S. J.; Kim, J.; Lee, J. S.; Min, D. H. A Graphene Oxide-Based Fluorescent Nanosensor to Identify Antiviral Agents Via a Drug Repurposing Screen. *Biosens. Bioelectron.* **2021**, *183*, 113208.

(24) Chandra, S.; Laha, D.; Pramanik, A.; Ray Chowdhuri, A.; Karmakar, P.; Sahu, S. K. Synthesis of Highly Fluorescent Nitrogen and Phosphorus Doped Carbon Dots for the Detection of Fe(3+) Ions in Cancer Cells. *Luminescence* **2016**, *31*, 81−87.

(25) Xie, Y.; Cheng, D.; Liu, X.; Han, A. Green Hydrothermal Synthesis of N-doped Carbon Dots from Biomass Highland Barley for the Detection of Hg2+. *Sensors* **2019**, *19*, 3169.

(26) Zhao, L.; Wang, Y.; Zhao, X.; Deng, Y.; Xia, Y. Facile Synthesis of Nitrogen-Doped Carbon Quantum Dots with Chitosan for Fluorescent Detection of Fe3+. *Polymers* **2019**, *11*, 1731.

(27) Liu, J.; Li, R.; Yang, B. Carbon Dots: A New Type of Carbon-Based Nanomaterial with Wide Applications. *ACS Cent. Sci.* **2020**, *6*, 2179−2195.

(28) Oh, Y. K.; Suh, D.; Kim, J. M.; Choi, H. G.; Shin, K.; Ko, J. J. Polyethylenimine-Mediated Cellular Uptake, Nucleus Trafficking and Expression of Cytokine Plasmid DNA. *Gene Ther.* **2002**, *9*, 1627−1632.

(29) Zhao, Q. Q.; Chen, J. L.; Lv, T. F.; He, C. X.; Tang, G. P.; Liang, W. Q.; Tabata, Y.; Gao, J. Q. N/P Ratio Significantly Influences the Transfection Efficiency and Cytotoxicity of a

Polyethylenimine/Chitosan/DNA Complex. *Biol. Pharm. Bull.* **2009**, *32*, 706−710.
(30) Xu, Z. Z.; Shen, G. B.; Xia, X. Y.; Zhao, X. Y.; Zhang, P.; Wu, H. H.; Guo, Q. F.; Qian, Z. Y.; Wei, Y. Q.; Liang, S. F. Comparisons of Three Polyethyleneimine-Derived Nanoparticles as a Gene Therapy Delivery System for Renal Cell Carcinoma. *J. Transl. Med.* **2011**, *9*, 46.
(31) Sk, M. P.; Chattopadhyay, A. Induction Coil Heater Prepared Highly Fluorescent Carbon Dots as Invisible Ink and Explosive Sensor. *RSC Adv.* **2014**, *4*, 31994−31999.

https://doi.org/10.1021/acsomega.3c01394
ACS Omega 2023, 8, 29113−29121